


Ultrafast carrier recombination in highly n-doped Ge-on-Si films

Cite as: Appl. Phys. Lett. **114**, 241104 (2019); <https://doi.org/10.1063/1.5088012>

Submitted: 07 January 2019 . Accepted: 07 June 2019 . Published Online: 20 June 2019

J. Allerbeck , A. J. Herbst, Y. Yamamoto, G. Capellini , M. Virgilio , and D. Brida 



View Online



Export Citation



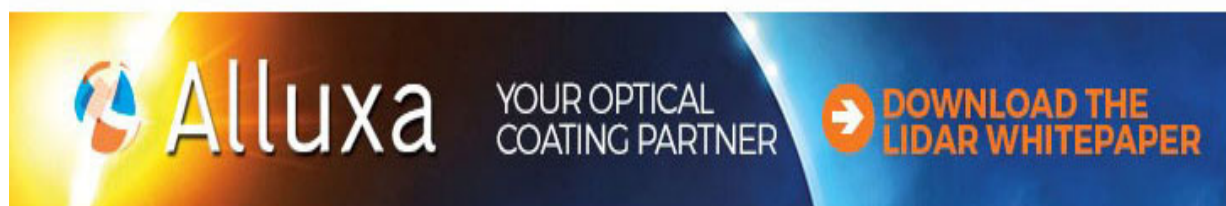
CrossMark

ARTICLES YOU MAY BE INTERESTED IN

[Efficient broadband terahertz generation from organic crystal BNA using near infrared pump](#)
Applied Physics Letters **114**, 241101 (2019); <https://doi.org/10.1063/1.5098855>

[Infrared luminescence from N-polar InN quantum dots and thin films grown by metal organic chemical vapor deposition](#)
Applied Physics Letters **114**, 241103 (2019); <https://doi.org/10.1063/1.5109734>

[Broadband nano-focusing of high-order harmonics in soft X-ray region with ellipsoidal mirror](#)
Applied Physics Letters **114**, 241102 (2019); <https://doi.org/10.1063/1.5091587>



Ultrafast carrier recombination in highly n-doped Ge-on-Si films

Cite as: Appl. Phys. Lett. **114**, 241104 (2019); doi: [10.1063/1.5088012](https://doi.org/10.1063/1.5088012)

Submitted: 7 January 2019 · Accepted: 7 June 2019 ·

Published Online: 20 June 2019







View Online



Export Citation



CrossMark

J. Allerbeck,¹  A. J. Herbst,¹ Y. Yamamoto,² G. Capellini,^{2,3}  M. Virgilio,⁴  and D. Brida^{1,5,a)} 

AFFILIATIONS

¹Department of Physics, University of Konstanz, D-78457 Konstanz, Germany

²IHP—Leibniz-Institut für innovative Mikroelektronik, Im Technologiepark 25, D-15236 Frankfurt (Oder), Germany

³Dipartimento di Scienze, Università di Roma Tre, V.le G. Marconi 446, I-00146 Roma, Italy

⁴Dipartimento di Fisica "E. Fermi," Università di Pisa, Largo Pontecorvo 3, I-56127 Pisa, Italy

⁵Physics and Materials Science Research Unit, University of Luxembourg, 162a avenue de la Faïencerie, L-1511 Luxembourg, Luxembourg

^{a)}Author to whom correspondence should be addressed: daniele.brida@uni.lu

ABSTRACT

We study the femtosecond carrier dynamics of n-type doped and biaxially strained Ge-on-Si films which occurs upon impulsive photoexcitation by means of broadband near-IR transient absorption spectroscopy. The modeling of the experimental data takes into account the static donor density in a modified rate equation for the description of the temporal recombination dynamics. The measurements confirm the negligible contribution at a high n-type doping concentration, in the 10^{19} cm^{-3} range, of Auger processes as compared to defect-related Shockley-Read-Hall recombination. Energy resolved dynamics reveal further insights into the doping-related band structure changes and suggest a reshaping of direct and indirect conduction band valleys to a single effective valley along with a significant spectral broadening of the optical transitions.

Published under license by AIP Publishing. <https://doi.org/10.1063/1.5088012>

After the pioneering papers envisaging a Ge/Si laser,^{1–5} a robust electrically pumped device has not been demonstrated yet. The working principle of the proposed laser leverages on the shallow energy barrier existing between the L_c -point and Γ_c minima in the conduction band of germanium. The original idea was to overcome this barrier by simultaneously exploiting a moderate tensile strain and heavy n-type doping to boost the photon emission rate in the optically active layer, as predicted theoretically.^{6,7} Despite the subsequent vast research effort put in place to target this goal, key aspects remain unsolved to date, in terms of both fundamental physics and technological issues. In fact, two main strategies have been proposed to enhance the net optical gain and hence enable practical applications.^{8,9} On one hand, researchers focused on increasing the strain^{10–12} with the recent demonstration of a low-threshold optically pumped laser based on intrinsic Ge nanowires. However, the exotic geometry usually featured by the active region has prevented the demonstration of an electrically pumped device. On the other hand, more conventional designs rely on low values of the strain, often limited to the thermal contribution typical of the Ge/Si heterostructures,¹³ but featuring a very high value of n-type doping density, typically beyond $1 \times 10^{19} \text{ cm}^{-3}$.^{14,15} However, the unsatisfactory results obtained using this type of material, such as the very high lasing threshold current, have prompted the quest for a

better understanding of the excess carrier dynamics in heavy-doped Ge. While it is generally accepted that Auger recombination is the dominant mechanism in moderately doped Ge ($< 1 \times 10^{18} \text{ cm}^{-3}$),^{16,17} its relative contribution to the total nonradiative recombination rate in the limit of high- or even ultrahigh donor densities is still in debate.^{18–20} In fact, recent studies suggest that high doping triggers a drastic reduction of the Shockley-Read-Hall (SRH) nonradiative recombination time τ_{SRH} in Ge/Si heterostructures, making this mechanism the one responsible for a reduced excess carrier density and, consequently, for an overall decrease in the photon emission rate.^{21–23} Nevertheless, other studies concluded that the presence of dopants in epitaxial Ge on Si has a negligible effect only on τ_{SRH} .²⁴

In this work, we perform time-resolved broadband transmission spectroscopy with intrinsic and ultrahigh doped epitaxial Ge/Si hetero-layers combined with theoretical modeling to assess the impact of donors on the recombination dynamics of optically excited carriers, generated after the absorption of near-IR photons across the direct gap. This work contributes to disentangle the different contributions controlling the nonradiative recombination in a wide range of excess carrier densities. Hereby, we provide experimental data that complement and enhance numerical simulation techniques.^{20,21} As a result, we underline the dominating influence of SRH processes over Auger

recombination in heavily doped Ge epilayers even in the limit of large Auger coefficients as reported in the literature.^{19,20}

Highly n-doped Ge/Si(001) films, featuring different phosphorous donor concentrations in the $1 \times 10^{19} \text{ cm}^{-3}$ range and a film thickness of approximately 800 nm, were grown by reduced pressure chemical vapor deposition²² on 8-inch Si wafers. An undoped sample (S0) grown in the same conditions and featuring a comparable crystal quality compared to the doped ones served as a benchmark to single out the influence of dopants. Background doping in the Ge layer was below 10^{15} cm^{-3} and below 10^{16} cm^{-3} in the silicon wafer (p-type), such that no observable physical effects can be linked to these low concentrations. The list of the samples employed in this study is reported in Table I, where we also show the energy of their direct bandgap $E_{G,PL}$, as measured by photoluminescence spectroscopy.²² The films exhibit 0.2% tensile strain due to the difference of the coefficient of thermal expansion existing between the Ge epilayer and the Si substrate. Optical polishing of the wafer backside enables broadband transmission measurements at photon energies below 1.1 eV (absorption by the silicon wafer), spanning over both the direct and indirect bandgaps of intrinsic Ge (at room temperature $E_{G,\Gamma} = 0.8 \text{ eV}$ and $E_{G,L} = 0.66 \text{ eV}$, respectively²⁵). In our experiments, we optically excite the Ge-on-Si films with femtosecond pulses and measure the energy-resolved (detection wavelength λ_D) differential transmission change $\Delta T/T(\Delta t, \lambda_D)$ around and below the intrinsic and effective bandgap as a function of the delay time Δt . A 190 nm Si_3N_4 antireflective coating at the sample backside enhances transmission of the probe pulse and avoids multiple excitations from pump pulse reflections. All measurements are performed at room temperature.

Figure 1(a) sketches the band structure of intrinsic Ge (iGe), summarizing the different excitation mechanisms together with thermalization and relaxation pathways. The experimental setup for time resolved spectroscopy is based on a Yb:KGW femtosecond laser that drives two home-made noncollinear optical parametric amplifiers (NOPAs) at a 50 kHz repetition rate.²⁶ One NOPA is tuned to a central wavelength of about $1.2 \mu\text{m}$ (1 eV photon energy) and serves as a pump pulse to excite direct interband transitions near the Γ -point with a fluence up to 2 mJ/cm^2 and a pulse duration of approximately 50 fs. The illumination spot size at the sample surface is approximately $500 \mu\text{m}$ in diameter. The second NOPA is spectrally tuned to cover a broadband range between 1.4 and $2.1 \mu\text{m}$ (0.6–0.85 eV) and set at a variable delay with respect to the pump pulse. Spectra of the complete series of pulses employed in the experiments are shown in Fig. 1(b). With this tuning of the pulses, the silicon substrate remains unperturbed during the measurement. After the interaction with the sample, the probe pulse is spectrally resolved with a monochromator (approximately 10 nm resolution) and detected with an extended-InGaAs

TABLE I. Intrinsic and heavily n-doped Ge-on-Si samples of 800 nm thickness employed in the experiments. The direct bandgap energy $E_{G,PL}$ is also reported.

Sample name	Donor density N_D (10^{19} cm^{-3})	$E_{G,PL}$ (meV)
S0	Intrinsic	770
S1	1.4	755
S2	2	745
S3	12 (50% active)	710

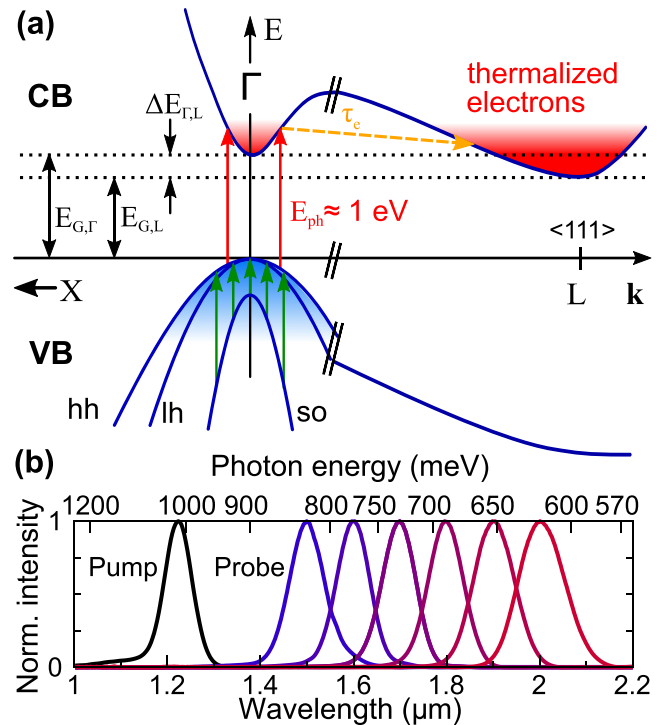


FIG. 1. (a) Schematic band structure of intrinsic Ge (blue curves) in the optically pumped state with interband photoexcitation indicated by red arrows. In the excited state, blue and red shaded areas depict thermalized holes and electrons, respectively. Intervalley scattering of electrons (τ_e , yellow dashed arrow) and photoinduced absorption (PIA, green arrows) occur in this configuration. (b) NOPA spectra used for pump and probe pulses.

photodiode. Pump modulation at 25 kHz allows high sensitivity and low noise single-shot boxcar detection. We vary the free space excitation fluence from low ($50 \mu\text{J/cm}^2$) to intermediate ($200 \mu\text{J/cm}^2$) and high (1.3 mJ/cm^2). The latter value corresponds to a saturation of the photocarriers according to a one photon absorption model derived by Mayer *et al.*²⁷ Our estimation of the photocarrier density therefore stands in contrast to much higher values obtained in other works.¹⁹

Figure 2 shows a reference measurement of transient absorption performed on the iGe film at an intermediate excitation level. Red and blue shaded regions indicate increased and decreased differential transmission, respectively. At the direct bandgap observable at $1.55 \mu\text{m}$ (0.8 eV), a sharp transition from the positive to negative signal occurs, which is associated with dynamic bandgap renormalization and its typical derivative spectral shape. This dominant feature is accompanied by a slightly increased differential transmission around $1.7 \mu\text{m}$ (0.74 eV) and broadband photoinduced absorption (PIA) at lower photon energies. The positive signal can be associated with renormalization and photobleaching of the indirect bandgap. The broadband negative signal occurring for photons with energies smaller than the indirect gap is due to the modulation of the refractive index of the photoexcited Ge. According to Carroll *et al.*,²⁸ PIA is dominated by optical transitions between split-off (SO) and heavy-hole (HH) valence bands, which become available in the optically excited state. The effective recombination time (evaluated along the dashed line in

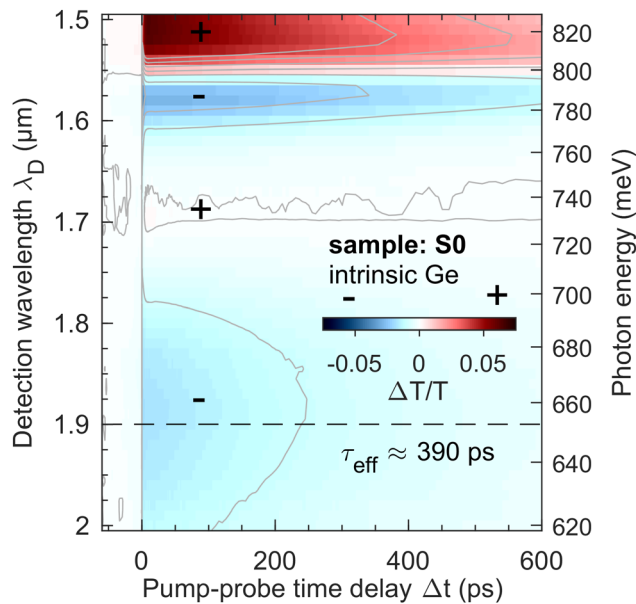


FIG. 2. Time and energy resolved differential transmission change $\Delta T/T$ from an undoped Ge-on-Si film at intermediate excitation fluence $\Phi = 0.2 \text{ mJ/cm}^2$. We estimate an unsaturated photocarrier density of $N_0 \approx 7 \times 10^{17} \text{ cm}^{-3}$. The dashed line at $1.9 \mu\text{m}$ shows a cut, along which the recombination time τ_{eff} is evaluated.

Fig. 2) reduces to few hundred picoseconds in thin films, while it is on the order of microseconds in the bulk crystal.^{24,29,30} This fast recombination is mediated by surface effects, lateral diffusion, and high electron temperatures, caused by an optical intensity during excitation on the order of a few gigawatts per centimeter square. At intermediate excitation pulse energy, electron thermalization and scattering from Γ_{CB} - to L_{CB} -valleys occur on sub- or few-picosecond time scales^{31,32} and can be neglected in the following analysis that considers only delay times $\Delta t > 5 \text{ ps}$. This is confirmed by our data and can be identified with the bending of contour lines near $\Delta t = 0$.

Differential transmission measurements as a function of pump-probe delay performed on doped Ge-on-Si films at the intermediate

excitation level are shown in Fig. 3. In comparison to the iGe reference film, we observe four significant effects: (1) the recombination time dramatically decreases with a higher doping concentration, (2) the transition between positive and negative signals spectrally redshifts and shows significant spectral broadening, (3) the optical signal associated with radiative transitions involving the L_{CB} and Γ_{CB} valleys cannot be distinguished in the doped samples, and (4) the maximum observed transmission change decreases with higher doping. Observation (1) is obvious as the density of defect centers increases with doping. Bandgap narrowing due to strain is also well known³³ and explains point (2). Optical spectra from doped layers usually feature a broad band where the peaks associated with indirect and direct transitions are less resolvable than in the intrinsic Ge case.²² In a band structure model, spectral broadening of optical transitions indicates the alignment of Γ_{CB} - and L_{CB} -valleys in the conduction band (CB).³⁴ Along this line, in our doped Ge samples, we observe an energy region spanning the direct and indirect bandgaps in which the differential transmission remains positive, hence hindering the distinction between the two radiative channels. In fact, since the photogenerated carrier density is much lower than the donor density, the dynamical renormalization of the direct gap is suppressed. As a consequence, the signal in both the direct and indirect gap regions remains positive, making impossible a distinction between these two processes, as found in (3). On the contrary, in iGe (Fig. 2), we observe a sharp energy region just below the direct gap where the differential transmission becomes negative. Below this photon energy band, we observe a positive differential transmission signal, caused by the bleaching of the indirect absorption, a signature of the energy difference between the valleys in Γ and L . In this context, the emission from possible radiative recombination is reabsorbed by free carriers that become available in the optically pumped state.²⁸ At low probe photon energy, PIA is the dominant effect providing the best energetic region to analyze carrier dynamics. Dashed lines indicate spectral cuts, along which the time constant of a single exponential decay fit is shown. Due to bandgap narrowing at higher donor densities and hence shifting of the spectral dynamics in different samples, we compare the recombination dynamics at the detection wavelength where the PIA contribution is the highest. At this probing energy, thermalization is extremely fast, as shown by the immediate decrease in the differential transmission signal after

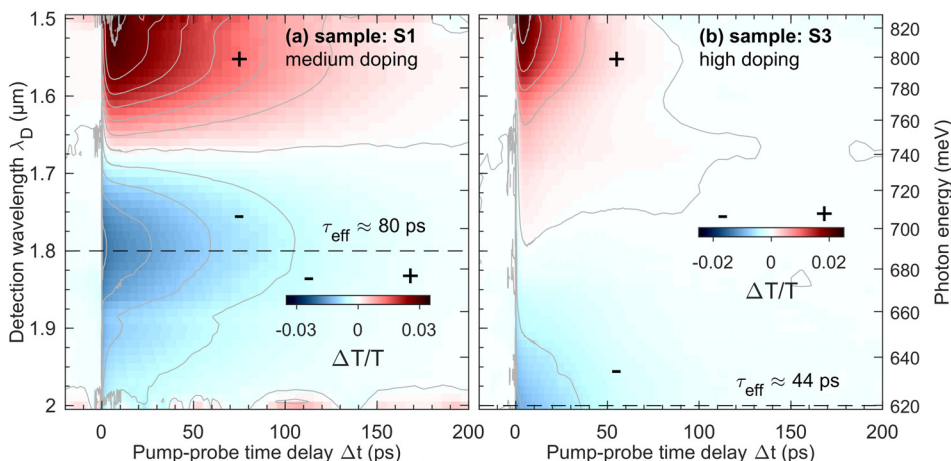


FIG. 3. Time and energy resolved differential transmission change $\Delta T/T$ from doped Ge-on-Si films (a) $N_D = 1.4 \times 10^{19} \text{ cm}^{-3}$ and (b) $N_D = 20 \times 10^{19} \text{ cm}^{-3}$ at intermediate excitation fluence $\Phi = 0.2 \text{ mJ/cm}^2$. We estimate an unsaturated photocarrier density of $N_0 \approx 7 \times 10^{17} \text{ cm}^{-3}$. The dashed line shows the recombination time at $1.8 \mu\text{m}$.

excitation [see contour lines in Figs. 3(a) and 2(b)]. At higher photon energies, where positive differential transmission indicates photo-bleaching of the Ge film, contour lines in Fig. 3 emphasize an increase in differential transmission within a few picoseconds after excitation, before recombination dynamics starts to dominate with a slower decrease in the pump-probe signal. Hence, the density of electrons at thermal equilibrium is the largest at a delay time of 5 ps, where the differential transmission becomes maximal. This thermalization signature becomes stronger at higher excitation densities (not shown), where the excited carriers display a larger excess energy. In contrast, the onset of the differential signal in regions of negative differential transmission is instantaneous and enables us to monitor carrier density even at short delay times. Regarding observation (4), a reduced differential transmission change at a high doping concentration also agrees with the increase in PL intensity.²²

We analyze the temporal dynamics of photocarrier recombination $N(\Delta t) \propto \Delta T/T(\Delta t)$ by fitting the experimental curves with rate equations that include Auger processes and defect-related Shockley-Read-Hall (SRH) recombination. While the nonradiative SRH rate associated with the crystal defect density describes single electron dynamics and is then linear in N , higher order Auger recombination also involves the static donor density N_D which scales as the equilibrium electron density, as illustrated in Fig. 4(a). This is expressed by the following rate equations:

$$\frac{dN}{dt} = -\gamma_{\text{SRH}}N - \dots$$

- (i) classic Auger process $\gamma_A N^3$,
- (ii) Auger with donors $\gamma_A N^2(N_D + N)$,
- (iii) Auger with high donor density $\gamma_A N(N_D + N)^2$,
- (iv) eff. single exponential ($N_D \gg N_0$) $\gamma_A N N_D^2$,

where $\gamma_{\text{SRH}} = 1/\tau_{\text{SRH}}$ describes the SRH recombination and γ_A is the Auger coefficient. In model (iv), we consider the scenario $N_D \gg N_0 = N(t=0)$, which yields a single exponential decay of $N(t)$ with effective time constant $\tau_{\text{eff}} = (\gamma_{\text{SRH}} + N_D^2 \gamma_A)^{-1}$. All models assume instantaneous excitation and do not incorporate excitation or nonthermal dynamics occurring times shorter than 5 ps.

In Fig. 4(b), the analytical solution of these rate equations is used to fit the measured recombination dynamics of sample S1 at intermediate and high carrier excitation densities. We spectrally integrate across the entire region that shows negative differential transmission to average all contributing PIA channels. For sample S1, this spectral region extends from $1.68 \mu\text{m}$ (0.74 eV) to $2 \mu\text{m}$ (0.62 eV) as found in Fig. 3(a). The estimated photocarrier densities at $\Delta t = 0$ ps are $N_{0,\text{int}} \approx 7 \times 10^{17} \text{cm}^{-3}$ and $N_{0,\text{high}} \approx 3 \times 10^{18} \text{cm}^{-3}$, respectively.²⁷ A lower limit of the fitting curves at 5 ps (vertical dashed line) ensures that only fully thermalized carriers contribute to the analysis. We applied models (i)–(iv) with small and large Auger coefficients from the literature to our data and show the relevant results in Fig. 4(b). Open fit parameters are an arbitrary amplitude and the SHR time constant τ_{SRH} , and the Auger coefficient and donor density are taken as fixed values. The blue fit (solid line) shows the dynamics of a single exponential decay according to model (iv). With a typical value for the Auger coefficient, this model corresponds to purely defect-related recombination. Red (dashed) and green (dotted) fits show the solution of model (ii) with small $\gamma_A = 10^{-31} \text{cm}^6/\text{s}$ (Ref. 35) and large

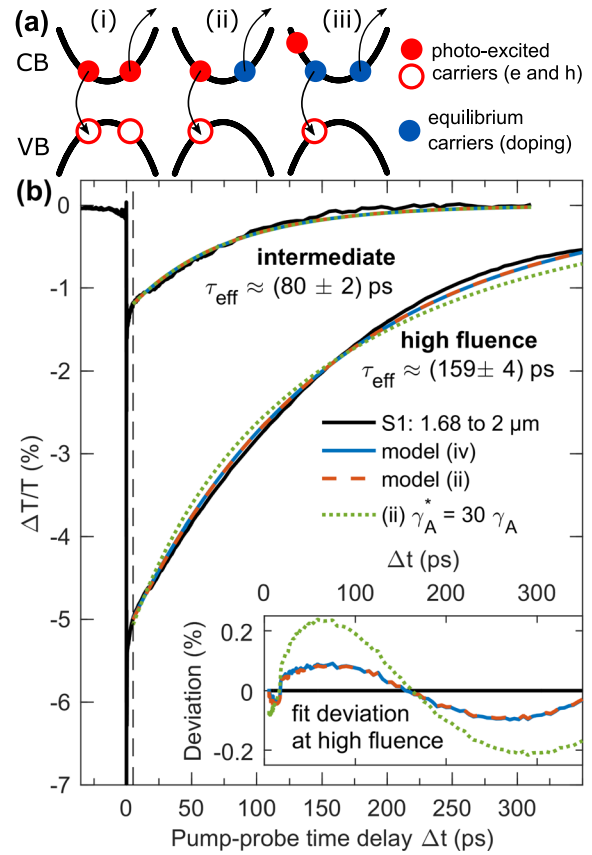


FIG. 4. (a) Schematic depiction of Auger recombination in a doped semiconductor. Three scenarios (i) intrinsic ($N_D = 0$), (ii) moderately doped ($N_D \approx N_0$), and (iii) highly doped ($N_D \gg N_0$) refer to fit models presented in the text. (b) Time resolved differential transmission signal $\Delta T/T$ obtained through spectral integration from $1.68 \mu\text{m}$ (0.74 eV) to $2 \mu\text{m}$ (0.62 eV) from sample S1 (black curves). The dynamics and fits are shown for intermediate and high excitation energy fluences Φ . Colored curves show the different fit models discussed in the text, and their deviation from the data is emphasized by the inset. In addition to a larger Auger coefficient, the dotted fit (green) assumes tenfold initial photocarrier density.

$\gamma_A^* = 3 \times 10^{-30} \text{cm}^6/\text{s}$ (Ref. 28) values for the Auger coefficient. To emphasize differences and exclude an error due to underestimation, the initial photocarrier density for the green fit is increased tenfold.

The classic Auger recombination model (i) remains indistinguishable from a single exponential decay (model iv) even for the larger Auger coefficient. Only for photocarrier densities much larger than 10^{19}cm^{-3} , which we consider unrealistic in our experimental conditions, it differs but also shows higher deviation from our data. Model (iii) yields a similar result to model (ii) with a modified Auger coefficient [$2\gamma_A^{(\text{iii})} = \gamma_A^{(\text{ii})}$], since contributions in the rate equation that correspond to models (i) and (iv) are negligible. In conclusion, the single exponential decay model (iv) approximates well our data. For reasonable values of the Auger coefficient, the effective recombination time constant can be identified with SHR processes: $\tau_{\text{eff}} \approx \tau_{\text{SRH}}$. This remains true also in different probing energy regions and for samples with different donor densities. Very large Auger coefficients or photocarrier densities diverge from the obtained recombination dynamics.

The recombination time increases linearly with the number of photocarriers according to our estimate,²⁷ which confirms our conclusion that Auger processes have a negligible contribution to the recombination of photocarriers. We note that at high probing energies with increased differential transmission, our models cannot capture the temporal dynamics of the recombination as well as for low energies. In the spectral region near the effective bandgap and at energies above, thermal effects, i.e. electron cooling, are more significant³⁶ and cause deviations from our simple recombination model. Thermalization processes in spectral regions with PIA are much faster as can be seen by the bending of contour lines in Fig. 3 for early delays and thus provide a better measure of the carrier lifetime. Nevertheless, the recombination time increases with carrier injection at all probing energies. Higher carrier densities can only be achieved through a significant contribution of two photon absorption at much shorter pulse length.²⁷

In conclusion, we performed time resolved differential transmission measurements on epitaxial Ge-on-Si films characterized by different levels of doping. To disentangle the effect of dopants on the photocarrier lifetime on the spot, their temporal dynamics is benchmarked with respect to an undoped reference sample grown with identical processing steps. We observed general changes in the energetic landscape and in the recombination dynamics of germanium with the reshaping of the Γ_{CB} - and L_{CB} -valleys in the conduction band at a high doping concentration. The broadened energetic signature of differential spectra measured in doped samples shows an energy overlap between the signals originating from Γ_{CB} - and L_{CB} -valleys. In addition, owing to a modeling that takes into account both static doping and optical excitation of free carriers, we determine that Auger processes do not dominate the carrier lifetime, which is instead limited by the SRH rate. The prevalence of this channel at high doping density is due to the increased crystal defect density, induced by the larger amount of dopants as also pointed out in Refs. 30 and 37. The significant shortening of the carrier lifetime with doping impurities is an obvious obstacle in the design of a potential germanium lasing device as suggested in Refs. 2, 3, 5, and 15. We show how looking at the energetic landscape and time resolved carrier dynamics in macroscopic Ge-on-Si structures from a fundamental semiconductor perspective benefits the understanding of this material system and its application potential.

This work was supported by the Emmy Noether Programm of the DFG (No. BR 5030/1-1).

REFERENCES

- J. Liu, X. Sun, D. Pan, X. Wang, L. C. Kimerling, T. L. Koch, and J. Michel, *Opt. Express* **15**, 11272 (2007).
- J. Liu, X. Sun, L. C. Kimerling, and J. Michel, *Opt. Lett.* **34**, 1738 (2009).
- X. Sun, J. Liu, L. C. Kimerling, and J. Michel, *Opt. Lett.* **34**, 1198 (2009).
- X. Sun, J. Liu, L. C. Kimerling, and J. Michel, *Appl. Phys. Lett.* **95**, 011911 (2009).
- J. Liu, X. Sun, R. Camacho-aguilera, C. Lionel, L. C. Kimerling, and J. Michel, *Opt. Lett.* **35**, 679 (2010).
- M. Virgilio, C. L. Manganelli, G. Grosso, G. Pizzi, and G. Capellini, *Phys. Rev. B* **87**, 235313 (2013).
- J. M. Escalante, *Opt. Mater.* **79**, 420 (2018).
- P. Boucaud, M. El Kurdi, A. Ghrib, M. Prost, M. de Kersauson, S. Sauvage, F. Aniel, X. Checoury, G. Beaudoin, L. Largeau, I. Sagnes, G. Ndong, M. Chaigneau, and R. Ossikovski, *Photonics Res.* **1**, 102 (2013).
- R. Geiger, T. Zabel, and H. Sigg, *Front. Mater.* **2**, 52 (2015).
- G. Capellini, C. Reich, S. Guha, Y. Yamamoto, M. Lisker, M. Virgilio, A. Ghrib, M. El Kurdi, P. Boucaud, B. Tillack, and T. Schroeder, *Opt. Express* **22**, 399 (2014).
- A. Elbaz, M. El Kurdi, A. Aassime, S. Sauvage, X. Checoury, I. Sagnes, C. Baudot, F. Boeuf, and P. Boucaud, *APL Photonics* **3**, 106102 (2018).
- S. Bao, D. Kim, C. Onwukaeme, S. Gupta, K. Saraswat, K. H. Lee, Y. Kim, D. Min, Y. Jung, H. Qiu, H. Wang, E. A. Fitzgerald, C. S. Tan, and D. Nam, *Nat. Commun.* **8**, 1845 (2017).
- G. Capellini, M. De Seta, P. Zaumseil, G. Kozłowski, and T. Schroeder, *J. Appl. Phys.* **111**, 073518 (2012).
- N. Higashitarumizu and Y. Ishikawa, *Opt. Express* **25**, 21286 (2017).
- R. Koerner, M. Oehme, M. Gollhofer, M. Schmid, K. Kostecki, S. Bechler, D. Widmann, E. Kasper, and J. Schulze, *Opt. Express* **23**, 14815 (2015).
- L. Hultdt, *Phys. Status Solidi* **8**, 173 (1971).
- N. G. Nilsson, *Phys. Scr.* **8**, 165 (1973).
- E. Gaubas and J. Vanhellemont, *J. Electrochem. Soc.* **154**, H231 (2007).
- T. T. Yeh, H. Shirai, C. M. Tu, T. Fuji, T. Kobayashi, and C. W. Luo, *Sci. Rep.* **7**, 40492 (2017).
- S. Dominici, H. Wen, F. Bertazzi, M. Goano, and E. Bellotti, *Appl. Phys. Lett.* **108**, 211103 (2016).
- D. S. Sukhdeo, S. Gupta, K. C. Saraswat, B. Dutt, and D. Nam, *Opt. Commun.* **364**, 233 (2016).
- M. R. Barget, M. Virgilio, G. Capellini, Y. Yamamoto, T. Schroeder, M. R. Barget, M. Virgilio, G. Capellini, and Y. Yamamoto, *J. Appl. Phys.* **121**, 245701 (2017).
- S. A. Srinivasan, C. Porret, M. Pantouvaki, Y. Shimura, P. Geiregat, R. Loo, J. Van Campenhout, and D. Van Thourhout, *Appl. Phys. Lett.* **113**, 161101 (2018).
- R. Geiger, J. Frigerio, M. J. Süess, R. A. Minamisawa, D. Chrastina, G. Isella, R. Spolenak, J. Faist, and H. Sigg, *Appl. Phys. Lett.* **104**, 062106 (2014).
- O. Madelung, *Semiconductors: Data Handbook* (Springer, Berlin, Heidelberg, 2004), ISBN: 978-3-642-18865-7.
- A. Grupp, A. Budweg, M. P. Fischer, J. Allerbeck, G. Soavi, A. Leitenstorfer, and D. Brida, *J. Opt.* **20**, 014005 (2018).
- B. Mayer, C. Schmidt, J. Bühler, D. V. Seletskiy, D. Brida, A. Pashkin, and A. Leitenstorfer, *New J. Phys.* **16**, 063033 (2014).
- L. Carroll, P. Friedli, S. Neuenschwander, H. Sigg, S. Cecchi, F. Isa, D. Chrastina, G. Isella, Y. Fedoryshyn, and J. Faist, *Phys. Rev. Lett.* **109**, 057402 (2012).
- D. T. Stevenson and R. Keyes, *J. Appl. Phys.* **26**, 190 (1955).
- E. Gaubas and J. Vanhellemont, *Appl. Phys. Lett.* **89**, 142106 (2006).
- X. Q. Zhou, H. M. Van Driel, and G. Mak, *Phys. Rev. B* **50**, 5226 (1994).
- G. Mak and W. W. Rühle, *Phys. Rev. B* **52**, R11584(R) (1995).
- R. Camacho-Aguilera, Z. Han, Y. Cai, L. C. Kimerling, and J. Michel, *Appl. Phys. Lett.* **102**, 152106 (2013).
- G. Grzybowski, R. Roucka, J. Mathews, L. Jiang, R. T. Beeler, J. Kouvetakos, and J. Menéndez, *Phys. Rev. B* **84**, 205307 (2011).
- R. Conradt and J. Aengenheister, *Solid State Commun.* **10**, 321 (1972).
- J. Frigerio, A. Ballabio, G. Isella, E. Sakat, G. Pellegrini, P. Biagioni, M. Bollani, E. Napolitani, C. Manganelli, M. Virgilio, A. Grupp, M. P. Fischer, D. Brida, K. Gallacher, D. J. Paul, L. Baldassarre, P. Calvani, V. Giliberti, A. Nucera, M. Ortolani, G. Pellegrini, P. Biagioni, C. Manganelli, V. Giliberti, and J. Frigerio, *Phys. Rev. B* **94**, 085202 (2016).
- J. Vanhellemont and E. Simoen, *Mater. Sci. Semicond. Process.* **15**, 642 (2012).